RSC Advances

PAPER

View Article Online
View Journal | View Issue

Cite this: *RSC Adv.*, 2025, **15**, 45136

Multi-layer encapsulation structures for stable bottom- and top-emitting white OLED devices

Ping-An Chen, Zian Yu, Hengjun Chen, Yifa Sheng, Chang Liu* and Xiaojun Li *

Organic light-emitting diode (OLED) devices have problems such as poor environmental stability, low thermal tolerance, and decomposition of materials. This work focuses on the encapsulation of white OLED devices with bottom and top emission. White OLED devices are realized by stacking tricolor luminescent materials as the light-emitting layer. The encapsulation structure is constructed with heat-conductive films, an inorganic barrier layer, liquid transparent glues, a POSS resin coating, and transparent films and glasses to solve stability problems. A three-dimensional protection system is constructed by multi-layer encapsulation, which consists of environmental isolation, a stress buffer, and thermal management. In addition, the highlight transmittance in either the bottom- or top-emitting directions is guaranteed by multiple transparent materials during encapsulation. The fabricated devices show white-light emission with an external quantum efficiency (EQE) of 11.6% for the top-emitting device and 7.5% for the bottom-emitting device. The decays of the encapsulated devices are significantly lower than those of unencapsulated devices, indicating that the designed encapsulation structures can improve the stability of the OLED devices. After 720 h, the encapsulated top- and bottom-emitting devices show a decay of about 20% and 16%, respectively. In contrast, the bright decay of the unencapsulated device exceeds 40%.

Received 21st September 2025
Accepted 4th November 2025

DOI: 10.1039/d5ra07156a

rsc.li/rsc-advances

Introduction

Organic light-emitting diodes (OLEDs) are one of the most common devices for displays; they are prepared by stacking electron and hole injection and transmission layers, a light-emitting layer, and electrodes, which are attached to the substrate. According to the substrate type, they can be categorized as rigid and flexible OLEDs, where rigid structures generally use an indium tin oxide (ITO) glass as the anode substrate and flexible structures use flexible films as the substrate.[1–4] OLED and micro/mini LED displays are self-luminous devices that have higher contrast, color gamut, and viewing angle than liquid crystal displays (LCDs).[5,6] LCDs are not self-luminous devices; they require a backlight module to provide light sources and liquid crystal conversion and filters to achieve the display. Micro/mini LED displays use a large number of LED beads to direct light emission, which need to be patched with point-to-point or mass transfer processes. Thus, OLEDs have a lower cost, simpler preparation process, low power consumption, and higher pixel resolution for display than micro/mini LEDs. Although OLED displays have many advantages over LED and LCD displays, they still suffer from poor stability. For instance, under the influence of external environmental factors, such as high temperature, stress, and exposure to water and oxygen, OLEDs are prone to degradation and oxidation due to the unstable organic materials.[7,8] The degradation of OLEDs can be attributed to factors such as ion migration, material deterioration, thermal decomposition, mechanical stress, hydrolysis, and oxidation. Therefore, effective mitigation of the influence of the external environment on OLEDs is key to the commercialization of OLEDs.

The impact of the external environment on OLED devices can be reduced to improve their stability through external encapsulation.[9–12] According to the light direction, OLEDs can be divided into two forms: top and bottom emission.[13–16] In bottom-emitting OLEDs, where light traverses the transparent substrate, the encapsulation's primary role is protection, with the substrate itself bearing the optical and mechanical responsibilities. Conversely, the transition to top-emitting OLEDs, which enable higher aperture ratios and superior contrast by emitting light through the top electrode, fundamentally redefines the encapsulation layer as a critical, multifunctional component. Here, encapsulation must simultaneously serve as a highly transparent optical window, a primary thermal dissipation pathway to manage heat from the opaque top electrode, and an ultra-robust barrier against moisture and oxygen to protect the sensitive organic layers. Therefore, the shift in emission direction elevates encapsulation from a relatively simple protective cover to an integral element whose optical clarity, thermal conductivity, and barrier performance are paramount to the device's overall efficiency, lifetime, and

School of Electrical Engineering, University of South China, Hengyang, 421001, China. E-mail: liuchang2046@163.com; lxj505873@163.com

viability in advanced applications such as high-resolution displays and flexible electronics.

In general, OLEDs are encapsulated in thin films or glasses, among which thin-film encapsulation (TFE) can achieve high compatibility with the miniaturization of OLEDs and has received extensive attention from researchers.[17,18] On one hand, the TFE can be modified through nanomaterials, optical structures, doping, and interface engineering. Choi *et al.* reported a multilayer thin-film-encapsulated OLED with Al_2O_3/SiO_xN_y/parylene-C, offering excellent protection and biocompatibility.[9] Yang *et al.* found that low elastic modulus and surface energy of TFE films can improve flexibility.[10] On the other hand, the use of a mixed film encapsulation layer composed of inorganic barriers and organic layers is a common strategy.[10,11] In general, UV-curing glass encapsulation is better than thermal curing for excellent environmental aging resistance, bonding strength, alignment precision, and manufacturing efficiency. Wu *et al.* designed multi-barrier thin-film encapsulation for OLEDs by depositing alternating layers of Al_2O_3 and parylene C.[18] Additionally, colorless polyimide film (CPI) or ultra-thin glass (UTG) as screen cover plates are used to improve scratch-, wear-, and impact-resistance.[19,20] However, research on TFE often only blocks the influence of a certain external environment and cannot simultaneously resist mechanical stress and block water and oxygen, while retaining high light transmittance and heat dissipation.

Herein, we report multi-layer encapsulation structures for top- and bottom-emitting white OLED devices. White light emission is achieved by stacking mixed blue-green and red light-emitting layers in the vertical direction. The encapsulation structure consists of multi-layer thin films, liquid optical glue sealing, and a transparent and hard coating. Mechanical stress, water, oxygen, and heat are resisted by the multi-layer encapsulation materials, while the light transmittance of the encapsulated device is retained above 82% compared with that of unencapsulated devices. This work focuses on the design and verification of top- and bottom-emission-based encapsulation structures for white OLED devices.

Experimental section

Device fabrication

The preparation and packaging processes of the unencapsulated OLED devices were carried out under vacuum conditions (1×10^{-5} to 5×10^{-6} torr). All coating and laminating processes were followed by defoaming and curing processes. The preparation process steps are as follows: (1) deposit anode on the glass or film substrate by vacuum vapor deposition with an evaporation rate of 2 Å s^{-1}. The substrate with TFT arrays was purchased from display material suppliers and was cleaned with ozone for 30 minutes and treated with oxygen plasma for 1 minute. (2) Deposit the hole injection and transport layers and the electron blocking layer with an evaporation rate of 0.1–0.5 Å s^{-1}. (3) Deposit the blue and green light-emitting layer, exciton buffer layer, and red light-emitting layer with an evaporation rate of 0.3 Å s^{-1}. (4) Deposit the hole blocking layer, ETL, and electron injection layer with an evaporation rate of 0.1–0.3 Å s^{-1}. (5) For bottom-emitting devices, deposit the cathode (Al_2O_3:Al) with an evaporation rate of 2 Å s^{-1}. For top-emitting devices, the cathode (Mg:Ag NWs solution) is spin-coated, then annealed at 150 °C for 30 minutes. (6) Light-curing epoxy resin glue is used to seal around the device. Finally, simple protection is applied to the devices. The unencapsulated structures of the bottom/top emitting OLED devices are shown in Fig. S1. For the unencapsulated structure of the bottom-emitting OLED, a SiO_2 thin film is deposited on the top side with an evaporation rate of 0.2 Å s^{-1}. For the unencapsulated structure of the top-emitting OLED, UTG is attached to the top side.

Device encapsulation

The encapsulation preparation process steps for the bottom-emitting devices are as follows: (1) place $CaCl_2$ desiccant with a particle size of 5–10 μm around the device, seal the device with OCR glue, then cure under UV light for 5 s. (2) Deposit the Al film on the surface of the OCR glue. Fit the heat-conductive adhesive on the Al deposition film and then bond the heat-conductive PI film. (3) The bottom transparent glass is bonded to UTG through OCA and then scrape-coated with POSS resin at 10 cm s^{-1}.

The encapsulation preparation process steps of the top-emitting devices are as follows: (1) place $CaCl_2$ desiccant around the device and seal the device with OCR glue. (2) Attach the UTG to the surface of the OCR glue. After UV curing for 5 s, the POSS resin is scrape-coated on the UTG with a speed of 10 cm s^{-1}. (3) Deposit a SiO_2 thin film on the bottom side with an evaporation rate of 0.2 Å s^{-1}, fit heat-conductive adhesive on the SiO_2 film, and then bond the heat-conductive PI film.

Characterizations

The *J–V–L* characteristics were recorded using a source measurement unit (2400 SourceMeter, Keithley Instruments) and a calibrated silicon photodiode. Efficiencies were calculated by assuming a Lambertian emission profile and by taking the measured angular emission profiles into account. Variations in device performance were measured by monitoring the relative luminance and current over time at a specific voltage using a source measurement unit and a silicon photodetector. The cross-sections of the encapsulated bottom- and top-emitting devices were examined with an optical microscope with 40× magnification, and the light was irradiated onto the sample from the bottom. The light transmittance was tested with a UV-visible spectrophotometer (UV-2600i). The light transmittance test was obtained by combining all encapsulation materials in the direction of light emission. All tests were conducted in an ambient environment.

Results and discussion

Structure and encapsulation of white OLED devices

According to the different directions of light emission, bottom- and top-emitting OLED devices were designed. Fig. 1a shows the structure of the bottom-emitting device, which consists of a transparent conductive substrate (100 nm ITO as anodes,

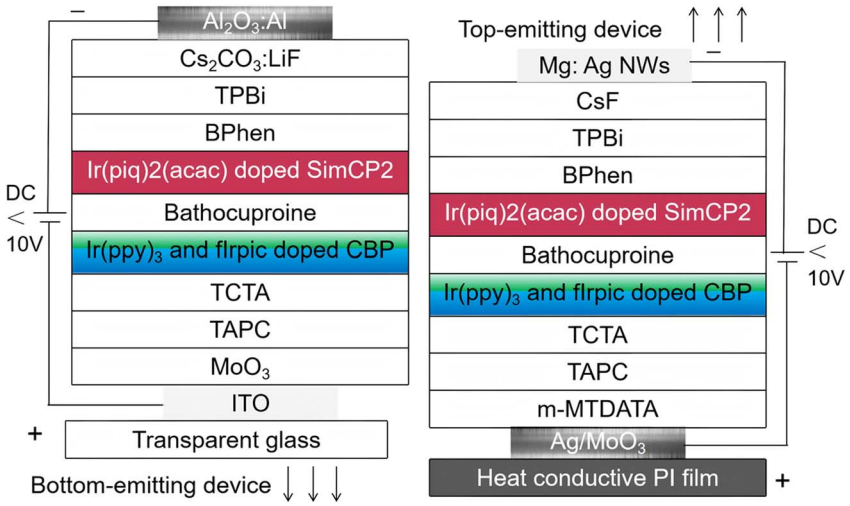

Fig. 1 Structures of the bottom- and top-emitting white OLED devices.

which are deposited on 900 μm glass, light transmittance > 90%), hole injection layer (5 nm MoO_3), hole transport layer (HTL, 50 nm TAPC, 1′-bis[4-(di-*p*-tolylamino)phenyl]cyclohexane), electron blocking layer (10 nm 4,4′,4″-tris(*N*-carbazolyl) triphenylamine, TCTA), blue and green light-emitting layer (30 nm, 3 wt% FIrpic and 4 wt% $Ir(ppy)_3$ doped 4,4′-bis(*N*-carbazolyl)-1,1′-biphenyl, CBP), exciton buffer layer (10 nm bathocuproine), red light-emitting layer (20 nm, 7 wt% $Ir(piq)_2(acac)$ doped SimCP2), hole blocking layer (5 nm BPhen), electron transport layer (ETL, 40 nm, 1,3,5-tris(1-phenyl-1*H*-benzimidazol-2-yl)benzene, TPBi), electron injection layer (1 nm Cs_2CO_3 and 1 nm LiF), and opaque metal cathode (5 nm Al_2O_3 deposited on 100 nm Al). The bottom-emitting device features an opaque metal with a low work function and high reflectivity as the cathode, and a transparent and conductive thin film anode. Since the top cathode is opaque and metal-reflective, the upward emitted light from the light-emitting layers is reflected back to the bottom anode, which converges with the downward emitted light, leading to less light loss. The electron blocking and exciton buffer layers prevent diffusion of electrons and excitons, respectively, which ensures that electrons and holes recombine within the light-emitting layer and reduces the non-radiative recombination losses.[21] The connection relationship of each part is that the transparent conductive film is the anode, and each functional layer is stacked in sequence through vacuum evaporation. Finally, the cathode material is evaporated on the electron injection layer.

Fig. 1b shows the structure of the top-emitting OLED device, which consists of a heat conductive polyimide (PI) film (100 μm), reflected anode (100 nm Ag/5 nm MoO_3), hole injection layer (20 nm, 4,4′,4″-tris(*N*-3-methylphenyl-*N*-phenylamino)triphenylamine, *m*-MTDATA), HTL (50 nm TAPC), electron-blocking layer (10 nm TCTA), blue and green light-emitting layer (30 nm, 3 wt% FIrpic and 4 wt% $Ir(ppy)_3$ doped CBP), exciton buffer layer (10 nm bathocuproine), red light-emitting layer (20 nm, 7 wt% $Ir(piq)_2(acac)$ doped SimCP2), hole blocking layer (5 nm BPhen), ETL (40 nm TPBi), electron injection layer (1 nm CsF), and transparent cathode (15 nm, 10% Mg doped Ag NWs). In order to ensure the top light emission of the device, the top is bare except for the semi-transparent Mg:Ag NWs anode, and the bottom is highly reflective.[22]

After encapsulation, the OLED device consists of the drive control layer on the substrate, the OLED device layer, and the encapsulation layer, as shown in Fig. 2. The drive control layer consists of a film or glass substrate, a control circuit composed of a TFT array and metal lines, a driver chip, and a flexible printed circuit (FPC) board that is bound to the substrate by an anisotropic conductive adhesive (ACF). The device layer consists of the OLED devices and framing glues with ultraviolet (UV) curing at the surrounding position. For the bottom-emitting device, the encapsulation layer consists of SiO_2 deposition film (20 nm), desiccant ($CaCl_2$), optical clear resin (OCR, 20 μm, light transmittance > 98%), Al deposition film (200 nm, light transmittance < 0.5%, thermal conductivity of 200 W m^{-1} K^{-1}), insulated heat conductive adhesive (100 μm, consists of acrylic adhesive, BN and additives, thermal conductivity 0.8 W m^{-1} K^{-1}) and insulated heat-conductive PI film (100 μm, BN modified PI with thermal conductivity of 3 W m^{-1} K^{-1}) at the top, optical clear adhesive (OCA, 25 μm, light transmittance > 95%), UTG with >92% transmittance (50 μm) and polyhedral oligomeric silsesquioxane (POSS) resin coating (20 μm, light transmittance > 91%) at the bottom. All raw materials are obtained from commercial sources. The SiO_2 film, desiccant, and OCR are used to isolate water and oxygen. The Al and heat-conductive PI films are used for heat dissipation and reflecting the light emitted from the device toward the top, back to the bottom. POSS-doped epoxy resin is a transparent coating with good hardness and adhesion that offers high resistance to scratching, wear, and impact. The POSS resin coating and transparent UTG are used to block water and oxygen, buffer mechanical stress, and provide the bottom light-emitting path. For the top-emitting device, the encapsulation layer consists of UTG (50 μm), desiccant ($CaCl_2$), optical clear resin (OCR, 20 μm), UTG (50 μm), POSS resin coating (20 μm) at the top, SiO_2 deposition

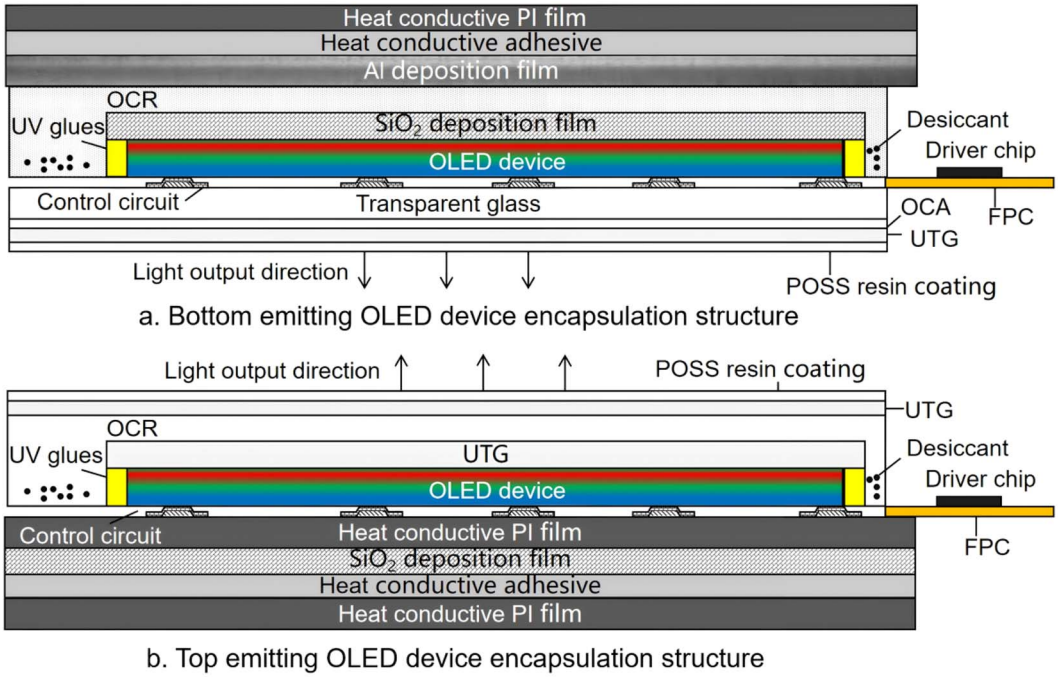

Fig. 2 Encapsulation structures of (a) bottom- and (b) top-emitting OLED devices.

film (20 nm), insulated heat conductive adhesive (50 μm), and heat conductive PI (200 μm) at the bottom.

In order to verify the multilayer integrity and bonding quality of the encapsulated devices, we used an optical microscope to observe the cross-section of the encapsulation layers (Fig. S2). The optical cross-sectional images exhibit a distinct hierarchical structure with different layers, and no obvious gaps between the different encapsulation layers, which further indicates that the encapsulation interface has good adhesion and integrity. The encapsulation of the bottom-emitting device focuses on top heat dissipation, light reflection, the water and oxygen barrier, and bottom transparent encapsulation. The encapsulation of the top-emitting device emphasizes optimized top light extraction efficiency and enhances heat dissipation and sealing through the bottom multi-layer barriers. Through the gradient change of the elastic modulus of encapsulation materials, external mechanical stress is attenuated layer by layer, and stresses during collision or pressing are absorbed, so as to prevent the functional layer from directly bearing overload. The degree of influence of the external environment on bottom/top-emitting OLED devices differs. Compared with the top-emitting device, the bottom-emitting device exhibits worse heat conduction on the substrate, while effectively preventing exposure to oxygen and water from the air through the OCR and glass layers, and it can withstand high mechanical stress due to the thick ITO glass.

Performance of the encapsulated white OLED devices

According to the designed structures, we fabricated bottom- and top-emitting OLED devices (see in the Experimental section). Fig. 3a shows the electroluminescence (EL) emission spectra of the top- and bottom-emitting OLED devices. Both devices exhibit multiple emission peaks in the regions of the three primary colors because their light-emitting layers are made of mixed blue, green and red organic light-emitting materials. Compared to the bottom-emitting devices, the multi-peak spectrum of the top-emitting OLED devices is more conducive to white light emission. The top-emitting device shows higher EL intensity and light transmittance than the bottom-emitting device. Bottom-emitting devices have low efficiency because the control circuits consist of a TFT array, and the metal lines on the bottom substrate reduce the effective light-emitting area.

Fig. 3b shows *J*–*V* curves of the top- and bottom-emitting OLED devices. In the low-voltage region (2.5–4.0 V), both current densities are extremely low, indicating that the device is in a weak trap filling restriction zone. The slope of the curve is close to 1, which conforms to Ohm's law characteristics, suggesting weak carrier mobility and injection capability.[15] With an increase in voltage, the slope gradually increases, indicating that the devices enter the space charge limited current (SCLC) region with low trap density, and high charge injection efficiency and transport capability. Compared with bottom-emitting devices, top-emitting devices require a lower voltage at the same brightness due to more efficient current injection, which can reduce power consumption. After encapsulation, the top-emitting and bottom-emitting devices retain 88% and 82% EL intensity, respectively. All encapsulation materials in the direction of light emission have a transmittance greater than 90%. The light transmittance of encapsulated devices remains above 82% (Fig. S3), indicating that the multi-layer encapsulation does not significantly sacrifice light transmittance while achieving device protection. In the top-emitting devices, the

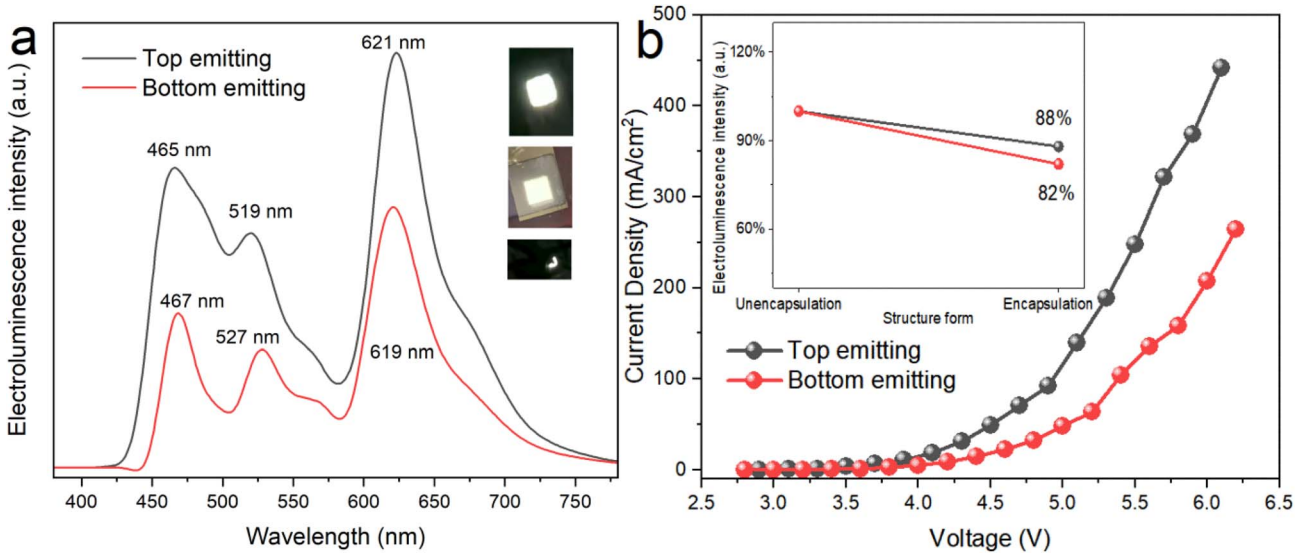

Fig. 3 (a) Electroluminescence emission spectra of top- and bottom-emitting OLED devices. (b) Current density–voltage (*J*–*V*) curves of top- and bottom-emitting OLED devices. The illustrations show illuminated encapsulated devices and the pressure test.

Mg:Ag NWs cathode has a low potential barrier for electron injection, and there is no metal absorption above the light-emitting layer, which reduces the loss of interface recombination after encapsulation.

Due to the larger light-emitting area, the top-emitting OLED device exhibits higher external quantum efficiency (EQE) than the bottom-emitting device, as shown in Fig. 4a. The EQE of both devices shows that they first rise to a peak and then decline as the current density increases. The top-emitting device has a maximum EQE of 11.6% and the bottom-emitting device has a maximum EQE of 7.5%. Efficiency improves due to the increase in the carrier concentration and the filling of defect states in the low current density region, while the efficiency roll-off occurs in the high current density region due to nonradiative recombination of excitons and thermal quenching. The top-emitting device exhibits faster efficiency roll-off in the high current density region than the bottom-emitting device because the electron–hole recombination region shifts, the cathode has relatively high resistivity, and micro-cavity resonance exacerbates carrier imbalance, resulting in high nonradiative recombination in top-emitting devices.[23] Top- and bottom-emitting OLED devices were packaged based on the designed encapsulation structures shown in Fig. 2. The encapsulation structures feature multi-layer TFE, liquid optical glue OCR sealing, and transparent and hard coating POSS. Fig. 4b shows the bright decay curves of the encapsulated and unencapsulated top- and

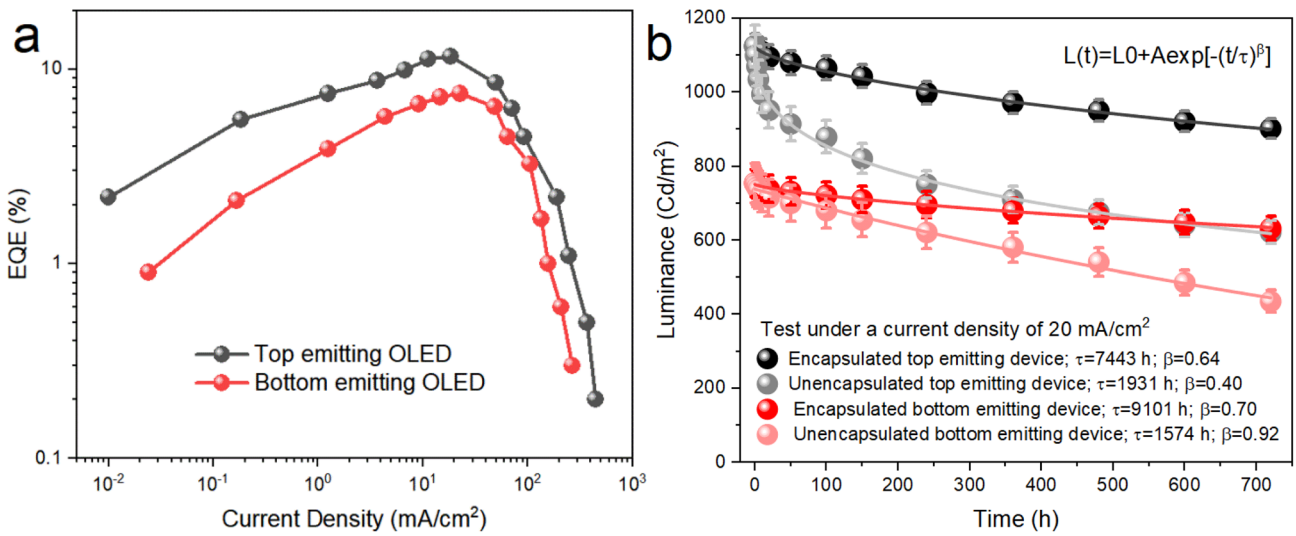

Fig. 4 (a) EQE of top- and bottom-emitting OLED devices. (b) Stability of the encapsulated and unencapsulated top- and bottom-emitting devices. Sample size is approximately 1.5 mm × 1.5 mm, the temperature is 25 °C, and the humidity is 70%.

bottom-emitting devices at a current density of 20 mA cm^{-2}, which reflect the luminescence stability of the devices. Based on the comparison of different devices, the encapsulated devices have 3–5% error bars, while the unencapsulated devices have 5–7% error bars. At the same time, we also calculated the characteristic decay time (τ) and stretch factor (β) of the devices using the stretching index model. The decay lifetime of the encapsulated devices is significantly larger than that of the unencapsulated devices (about 4 times for the top-emitting device, 6 times for the bottom-emitting device), indicating that the designed encapsulation structures can improve the stability of the OLED devices. The brightness of the encapsulated top-emitting device remains above 900 cd m^{-2} after 720 h, with a decay of about 20%, while that of the bottom-emitting device is about 16%. The bottom-emitting devices have better stability because they effectively prevent exposure to oxygen and water from the air through both the OCR and glass layers. However, the unencapsulated devices exhibit the fastest decay, exceeding 40%.

Fig. 5a presents the power efficiency *versus* luminance for the two types of OLEDs. Maximum power efficiencies of 61.4 and 31.5 lm W^{-1} were achieved for the top- and bottom-emitting OLEDs, respectively. Across the luminance range from 10^1 to 10^4 cd m^{-2}, both OLED configurations show a decline in power efficiency with increasing luminance. The bottom-emitting OLED consistently exhibits higher power efficiency than the top-emitting OLED over the entire tested luminance range. The top-emitting device exhibits higher EQE but lower power efficiency than the bottom-emitting device. This difference likely stems from structural factors, such as charge imbalance, low light extraction efficiency, nonradiative recombination, high metal electrode resistance, high waveguide mode, and interface loss in the top-emitting device, which allow high photon conversion efficiency but low current and light extraction efficiencies.

Fig. 5b illustrates the relationship between current efficiency (cd A^{-1}) and current density (mA cm^{-2}) for the OLEDs. As the current density increases, the current efficiency of the bottom-emitting device rapidly decreases, while the current efficiency of the top-emitting device first stabilizes and then slowly decreases. Across the entire range of current densities shown, the bottom-emitting OLED consistently has a higher current efficiency than the top-emitting OLED. The bottom-emitting device has small waveguide loss, due to the low light reflection and refraction loss at the ITO and air interfaces, which enhances the current efficiency. The high current density leads to a sharp increase in exciton concentration, which, in turn, causes a dramatic rise in non-radiative recombination processes such as triplet–triplet annihilation (TTA) and singlet–singlet annihilation (SSA), resulting in a sudden drop in luminescence efficiency. Meanwhile, under high current conditions, the thermal effect of the top metal electrode accelerates the non-radiative decay of excitons, further reducing the efficiency. In the top-emitting device, the internal electric field distribution is favorable for carrier balance and low exciton quenching rate because both ends are equipped with metal electrodes, which exhibit a gradual efficiency decline under high current densities.[24]

The chromaticity coordinates of the top- and bottom-emitting devices at different working voltages are summarized in the chromaticity diagram shown in Fig. 6a. Compared with bottom-emitting OLEDs, the chromaticity coordinates of top-emitting OLEDs are more concentrated in the white region that is close to the white light perceived by human eyes. The multiple transparent encapsulation layers of the top-emitting OLEDs will cause light interference effects, resulting in the "stretching" of narrowband spectra generated by exciton recombination into broadband spectra, and showing the aggregation of color coordinates toward the white region. The bottom-emitting OLED emits light from the ITO substrate, and the interlayer interference effect is weak; the device shows an

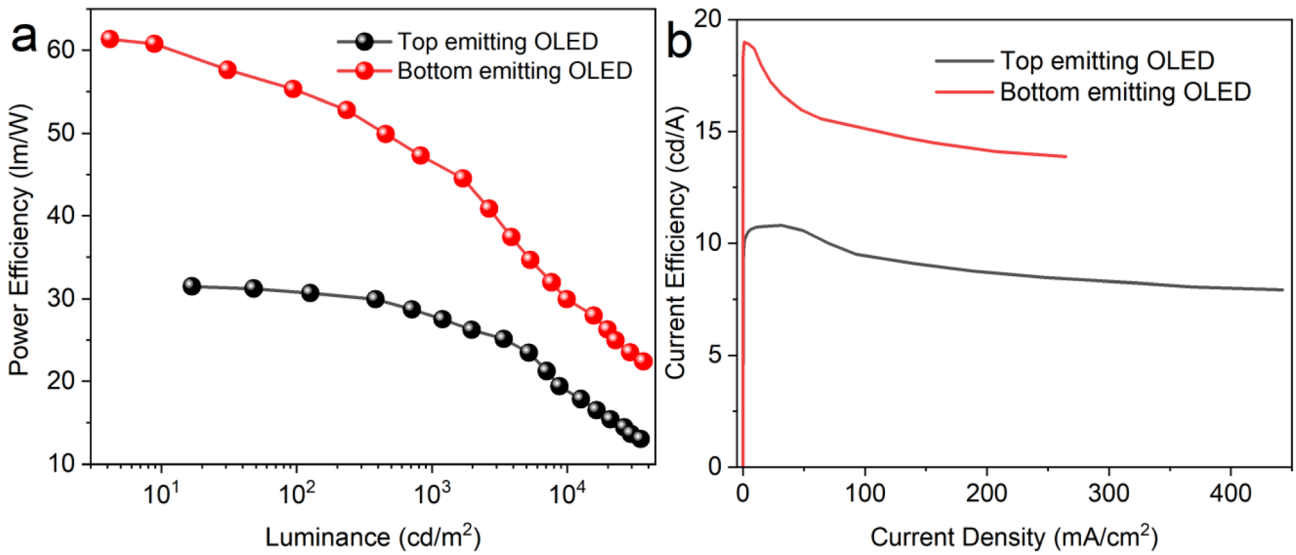

Fig. 5 (a) Power efficiency as a function of luminance; (b) current efficiency *versus* current density.

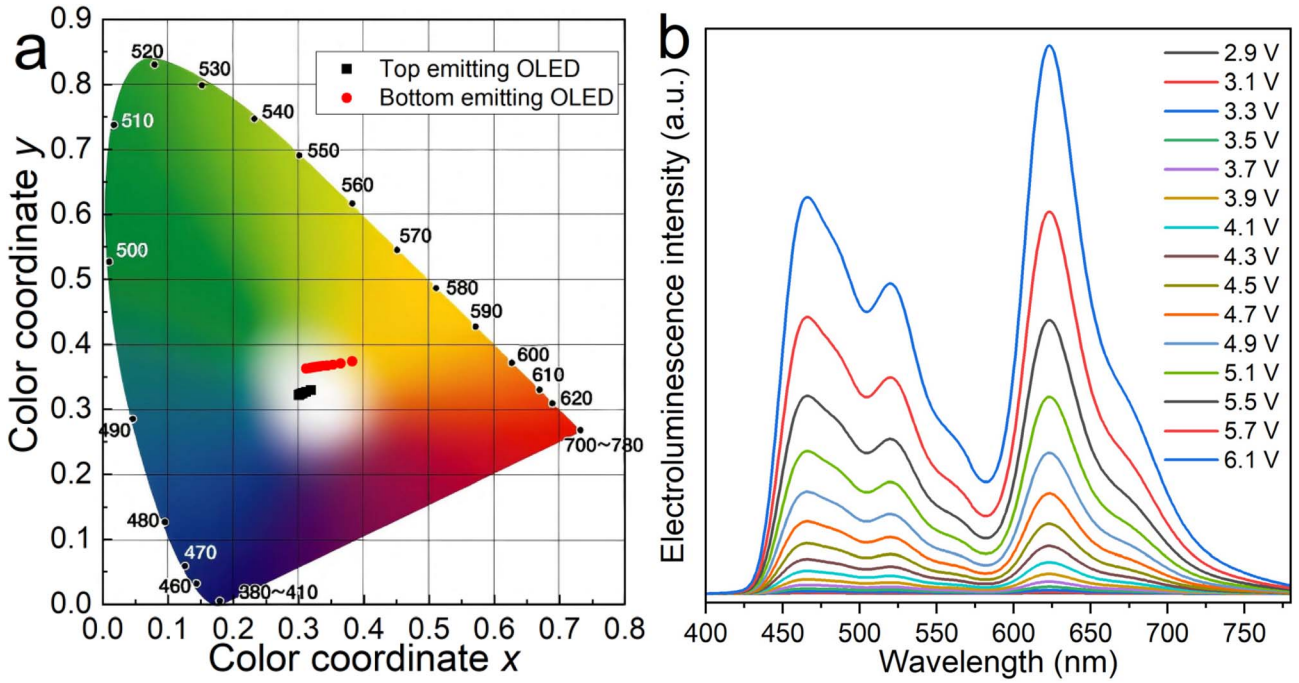

Fig. 6 (a) Chromaticity coordinates of top- and bottom-emitting OLEDs at different working voltages within the range of 2.8–6.2 V; (b) electroluminescence emission spectra of top-emitting OLED at different working voltages.

intrinsic narrowband spectrum that is generated by exciton recombination, high color purity, and a shift away from the white region. Fig. 6b shows the EL emission spectra of the top-emitting OLED at different working voltages. As the working voltage increases, the EL intensity gradually rises, while the emission peak shows no significant change, indicating that the device has excellent voltage stability.

The light-emitting layers and electrodes of the unencapsulated devices are easily permeated by water and oxygen, resulting in material degradation, such as oxidation of organic

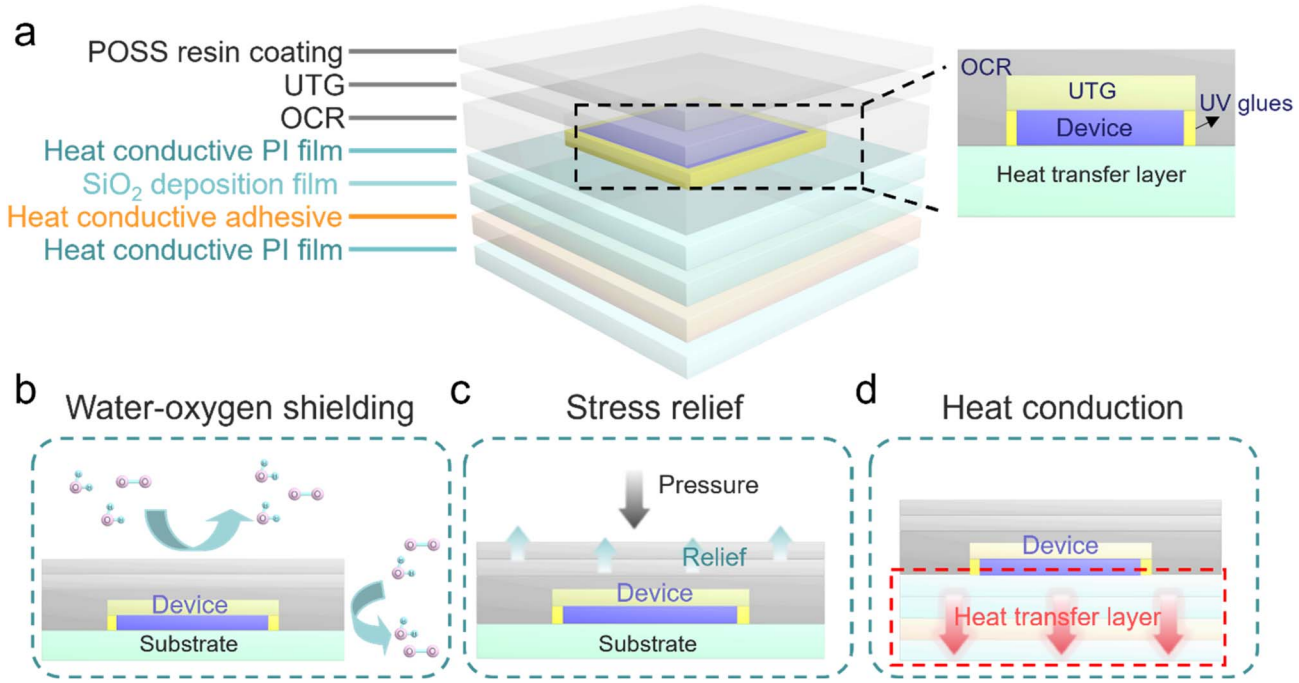

Fig. 7 (a) Schematic of the device structure, and diagrams of (b) water–oxygen shielding, (c) stress relief, and (d) heat conduction.

molecules and corrosion of the electrodes.[25,26] The degradation mechanism of these devices mainly originates from stress, water, oxygen, and heat. Therefore, multiple inorganic and organic composite barrier layers in and out of the device are constructed to significantly enhance its stability, as shown in Fig. 7a. To reduce the penetration of water and oxygen, the device uses multiple barrier layers and is sealed with liquid glue (UV glue), as shown in Fig. 7b. After curing, the liquid glues form a non-porous elastic sealing layer that fills the gap at the edge of the device and prevents water vapor from invading from the side. The penetration of water and oxygen is blocked by a dense film and glue structure, with trace amounts of permeated water vapor chemically adsorbed by $CaCl_2$, and the low surface energy properties of UTG and POSS reduce water vapor adhesion (for detailed discussions, see the SI). Secondly, multiple encapsulation materials are also used to improve the mechanical and heat dissipation performances of devices, as illustrated in Fig. 7c. The stress buffer depends on the gradient elastic modulus of the different encapsulation layers. The stress blocking mechanism is that the POSS coating provides flexible buffering and wear resistance, the UTG offers rigid support to restrict deformation and cracks, and the OCR disperses stress through high elastic modulus. The CPI, OCA, OCR, and POSS resin coatings have high light transmittance (>90%) and can achieve both packaging and light transmission functions. The pressure test (illustration in Fig. 3a) indicates that the luminance intensity of the device remains at 95% after 500 pressure cycles at 50 N. The excellent stress tolerance is attributed to the generated mechanical stress being absorbed by the multi-layer films and the elastic glue layers.

Thirdly, the heat energy transfers from the light-emitting layers to the encapsulation layer. The Al deposition film and insulated heat-conductive PI film accelerate the conduction of heat from the inside to the outside, as shown in Fig. 7d. The top-emitting device is susceptible to encapsulation because the anode Ag is more prone to diffusion, the semi-transparent cathode (Ag:Mg) is liable to generate heat, and the encapsulation layer affects the microcavity effect, thereby reducing light extraction efficiency. The bottom-emitting device has inert electrodes without ion migration and heat generation, but this comes at the expense of aperture ratio. The initial rapid decay of the OLED devices is attributed to the activation of defects, which form non-radiative recombination centers. Then, the devices enter a slow exponential decay stage that is caused by exciton–electrode interaction and triplet–triplet annihilation. Therefore, the multi-dimensional composite encapsulation layers simultaneously ensure the stability, light transmittance, and heat dissipation performance of the device.

Conclusion

In summary, we designed encapsulation structures with multi-layer materials for bottom- and top-emitting white OLED devices to improve their stability. This work provides new design philosophies and direction-dependent optimization for OLED encapsulation; these include multiple environmental factors, the contradiction between encapsulation and light transmittance, and encapsulation strategies for devices with different emission directions. The issues of water and oxygen erosion, thermal failure, and mechanical brittleness in OLED devices are systematically addressed by multi-dimensional collaborative encapsulation. The inorganic barrier layer, thermal conductive substrate, sealing glues, reflectors, transparent hard coating, and UTG together allow the construction of a three-dimensional protection system of environmental isolation, stress buffering, and thermal management. In addition, the highlight transmittance in either the bottom- or top-emitting directions is guaranteed during encapsulation. The results indicate that the designed encapsulation structures can significantly improve the stability of the OLED devices. Compared with bottom-emitting devices, top-emitting devices exhibit higher luminescence intensity due to their larger effective light-emitting area. While bottom-emitting devices are superior to top-emitting devices because of their improved stability through encapsulation. This research provides guidance for the design and encapsulation of OLED devices with different light-emitting directions.

Author contributions

The manuscript was written by Ping-An Chen, Xiaojun Li is the first corresponding author and proposed innovative ideas and experimental designs. Xiaojun Li, Zian Yu and Hengjun Chen are responsible for data collection and testing. The manuscript was revised by Yifa Sheng. Xiaojun Li and Chang Liu provide funding support and guidance. All authors have given approval to the final version of the manuscript.

Conflicts of interest

All the authors declare that they have no known competing financial interests or personal relationships that could have appeared to influence the work reported in this manuscript.

Data availability

Data will be available from the corresponding author upon request.

Supplementary information: unencapsulated structure, optical microscopy images of device cross section, transmittance of encapsulation layer in the light emitting direction and material characteristics. See DOI: **https://doi.org/10.1039/d5ra07156a**.

Acknowledgements

This work was supported by the National Key Research and Development Project funding from the Ministry of Science and Technology of China (2022YFE0118400), the National Natural Science Foundation of China (Grant No. 62174078), the Natural Science Foundation of Hunan Province (Grant No. 2022RC1076 and 2023JJ40554), the Doctoral Research Start-up Foundation of University of South China (5525QD015).

References

1 J. Song, H. Lee, E. G. Jeong, K. C. Choi and S. Yoo, *Adv. Mater.*, 2020, **32**, 1907539.
2 G. Gustafsson, Y. Cao, G. M. Treacy, F. Klavetter, N. Colaneri and A. J. Heeger, *Nature*, 1992, **357**, 477–479.
3 X.-Y. Zeng, Y.-Q. Tang, X.-Y. Cai, J.-X. Tang and Y.-Q. Li, *Mater. Chem. Front.*, 2023, **7**, 1166–1196.
4 M. Godi, H. Kwon, S. Park, S. Park, H. Lee, K. Lee and J. Park, *RSC Adv.*, 2024, **14**, 8135–8144.
5 H.-W. Chen, J.-H. Lee, B.-Y. Lin, S. Chen and S.-T. Wu, *Light: Sci. Appl.*, 2018, **7**, 17168.
6 Y. Huang, E.-L. Hsiang, M.-Y. Deng and S.-T. Wu, *Light: Sci. Appl.*, 2020, **9**, 105.
7 E. Tankelevičiūtė, I. D. W. Samuel and E. Zysman-Colman, *J. Phys. Chem. Lett.*, 2024, **15**, 1034–1047.
8 J.-S. Park, H. Chae, H. K. Chung and S. I. Lee, *Semicond. Sci. Technol.*, 2011, **26**, 034001.
9 S. Choi, J. W. Park, H. Cho, J.-W. Shin, K. Kim, O. E. Kwon, J.-H. Yang, C.-M. Kang, C.-W. Byun and S.-D. Jung, *ACS Appl. Mater. Interfaces*, 2025, **17**, 25534–25545.
10 H. I. Yang, K. R. Naveen, S. M. Cho, J. Y. Kim, Y. H. Jung and J. H. Kwon, *Org. Electron.*, 2023, **115**, 106761.
11 Y. Weng, G. Chen, X. Zhou, Y. Zhang, Q. Yan and T. Guo, *ACS Appl. Polym. Mater.*, 2023, **5**, 10148–10157.
12 A. P. Ghosh, L. J. Gerenser, C. M. Jarman and J. E. Fornalik, *Appl. Phys. Lett.*, 2005, **86**, 223503.
13 T.-Y. Chu, J.-F. Chen, S.-Y. Chen, C.-J. Chen and C. H. Chen, *Appl. Phys. Lett.*, 2006, **89**, 053503.
14 M.-H. Lu, M. S. Weaver, T. X. Zhou, M. Rothman, R. C. Kwong, M. Hack and J. J. Brown, *Appl. Phys. Lett.*, 2002, **81**, 3921–3923.
15 M. Huang, Z. Chen, J. Miao, S. He, W. Yang, Z. Huang, Y. Zou, S. Gong, Y. Tan and C. Yang, *Nat. Commun.*, 2024, **15**, 8048.
16 H. Xiang, R. Wang, J. Chen, F. Li and H. Zeng, *Light: Sci. Appl.*, 2021, **10**, 206.
17 Y. Jeon, H. Lee, H. Kim and J.-H. Kwon, *Micromachines*, 2022, **13**, 1478.
18 J. Wu, F. Fei, C. Wei, X. Chen, S. Nie, D. Zhang, W. Su and Z. Cui, *RSC Adv.*, 2018, **8**, 5721–5727.
19 C. Yi, W. Li, S. Shi, K. He, P. Ma, M. Chen and C. Yang, *Sol. Energy*, 2020, **195**, 340–354.
20 M.-H. Ha, J.-K. Choi, B.-M. Park and K.-Y. Han, *J. Mech. Sci. Technol.*, 2021, **35**, 661–668.
21 S. H. Kim, J. Jang and J. Y. Lee, *Appl. Phys. Lett.*, 2007, **90**, 223505.
22 S.-K. Kwon, E.-H. Lee, K.-S. Kim, H.-C. Choi, M. J. Park, S. K. Kim, R. Pode and J. H. Kwon, *Opt. Express*, 2017, **25**, 29906–29915.
23 J. Jiang, W. Zheng, J. Chen, Z. Xu, D. Song, B. Qiao and S. Zhao, *Molecules*, 2020, **25**, 2867.
24 Z. Wang, Y. Xi, Z. Liang, X. Tan, D. Xu and W. Chen, *Optoelectron. Lett.*, 2023, **19**, 385–390.
25 C. Keum, C. Murawski, E. Archer, S. Kwon, A. Mischok and M. C. Gather, *Nat. Commun.*, 2020, **11**, 6250.
26 S. Scholz, D. Kondakov, B. Lüssem and K. Leo, *Chem. Rev.*, 2015, **115**, 8449–8503.